Terbit *online* pada laman web jurnal : http://metal.ft.unand.ac.id

METAL: Jurnal Sistem Mekanik dan Termal

| ISSN (Print) 2598-1137 | ISSN (Online) 2597-4483 |

Research Article

Experimental Investigation and CFD Simulation of the Thermal Performance of a direct Solar Fish Dryer Integrated with Phase Change Material for Salted Fish Drying

Emil Mahfuzi[a], *Azridjal Aziz*[a], *Rahmat Iman Mainil*[a]

[a]*Department of Mechanical Engineering, Universitas Riau, Pekanbaru, Indonesia*

ARTICLE INFORMATION

Article History:
Received: 27 Agustus 2026
Revised: 28 October 2026
Accepted: 30 October 2026

KEYWORDS

CFD
Direct solar fish dryer
Phase Change Material
Thermal energy storage
Thermal performance

CORRESPONDENCE

E-mail: azridjal.aziz@lecturer.unri.ac.id

A B S T R A C T

Solar drying is a sustainable preservation technology for fish products; however, its performance is limited by fluctuations in solar radiation, resulting in unstable drying temperatures and inconsistent product quality. This study experimentally investigated the thermal performance of an direct trapezoidal solar fish dryer integrated with paraffin-based Phase Change Material (PCM) and CFD simulation for drying salted ikan sepat (Trichopodus trichopterus). Comparative experiments were conducted on dryers with and without PCM (WOPCM) under natural outdoor conditions. Chamber temperatures were monitored using sixteen temperature sensors, while solar radiation, ambient humidity, airflow velocity, and fish weight were continuously recorded throughout the drying process. The experimental results demonstrated that the PCM-assisted dryer maintained a more stable thermal environment during periods of declining solar radiation because the paraffin wax released the latent heat stored during peak sunshine. Although the maximum chamber temperature of both systems was comparable during peak solar intensity, the PCM-integrated dryer exhibited a slower temperature decay after sunset and prolonged the effective drying period. Continuous weight measurements confirmed progressive moisture removal throughout the drying process, indicating that the stored thermal energy contributed to maintaining drying conditions beyond periods of direct solar heating. These findings demonstrate that integrating PCM into an direct solar fish dryer enhances thermal stability and operational continuity, making it a promising renewable-energy technology for improving the reliability of small-scale salted fish drying.

1. INTRODUCTION

Solar drying is a promising approach for reducing energy consumption in conventional food-drying processes by utilizing renewable solar energy. It is particularly relevant for agricultural and fishery products, for which drying is an important preservation method. However, the performance of solar dryers is strongly influenced by fluctuations in solar radiation and ambient conditions, which can cause variations in drying-air temperature and reduce the continuity of the drying process. Thermal energy storage (TES) has therefore attracted considerable attention as a means of improving the thermal performance of solar thermal technologies. Phase change materials (PCMs) are particularly attractive for TES applications because they can store and release substantial amounts of latent heat within a relatively narrow temperature range[1] Recent research has investigated PCM integration in solar dryers and related thermal systems to

https://doi.org/ 10.25077/metal.10.2.124-137.2026

This is an Open Access article distributed under the terms of the Creative Commons Attribution-NonCommercial-ShareAlike 4.0 International License

improve heat utilization and maintain thermal performance under variable solar conditions [2]

Previous studies have examined different thermal storage approaches and PCM configurations for solar drying applications. [3]compared sensible- and latent-heat storage in a small-scale solar thermal dryer, demonstrating the relevance of selecting an appropriate thermal storage mechanism for dryer performance. [4] investigated the effects of PCM positioning within a solar collector, highlighting the importance of storage location in the thermal design of solar dryers. [5] evaluated an indirect cabinet solar dryer equipped with PCM through life-cycle assessment, energy analysis, and exergy analysis. Other investigations have extended PCM integration to photovoltaic–thermal and greenhouse drying systems, including assessments of thermal performance, environmental impacts, and economic considerations [6]. These studies indicate that the effectiveness of PCM-assisted solar drying depends not only on the thermophysical properties of the storage material but also on its integration into the overall thermal system.

Research into PCM materials and heat-transfer configurations has also expanded beyond conventional solar dryers. [7] investigated form-stable PCM composites using aligned-channel gelatin–nanographite aerogels for solar-thermal energy conversion and storage. [8] evaluated the energetic and exergetic performance of a double-pass solar air collector incorporating fins and PCM. [9] examined the thermal storage layer of a solar air collector by considering multiple PCM-related design factors, while [10] numerically investigated different PCM container configurations for solar dryer applications. Studies on passive and active indirect solar dryers have further evaluated the use of PCM during the drying of ivy gourd [11]. In related photovoltaic–thermal applications, [12] reviewed design approaches for implementing PCM to regulate system temperature. [13] also conducted energy, exergy, exergoeconomic, and exergo-environmental analyses of a large-scale solar dryer with PCM thermal storage. Collectively, these investigations emphasize the importance of PCM placement, container geometry, heat-transfer pathways, and system-level performance evaluation.

Further developments in solar air heating and thermal storage provide additional insights into the design of PCM-assisted drying systems. [14] investigated the optimization of a solar air heater incorporating PCM for drying applications. [15] experimentally studied and optimized a passive bifacial photovoltaic–thermal greenhouse dryer integrated with PCM. Although some research has focused on other solar-thermal applications, such as PCM-assisted solar desalination [16] and PCM-embedded pyroelectric systems for solar energy harvesting, these studies illustrate broader approaches to utilizing and managing solar energy. Similarly, [17] investigated graphene-doped polyvinyl alcohol aerogel composites for photothermal conversion and solar-energy storage. Nevertheless, material-level advances.

2. MATERIALS AND METHODS

An experimental and numerical investigation was conducted to evaluate the thermal performance of a direct solar fish dryer integrated with phase change material (PCM) for salted-fish drying. The study combined outdoor drying experiments with computational fluid dynamics (CFD) simulations to characterize the coupled heat and airflow behavior inside the drying chamber. The experimental investigation was performed under natural solar radiation, while the CFD model was developed to predict the temperature distribution, airflow characteristics, and heat-transfer behavior within the dryer.

The overall research procedure consisted of five main stages: (i) design and fabrication of the solar fish dryer; (ii) characterization and integration of the PCM thermal-storage system; (iii) experimental drying tests with and without PCM; (iv) development and validation of the CFD model; and (v) comparative evaluation of the thermal performance and drying characteristics.

2.1. Materials

Salted ikan sepat (Trichopodus trichopterus) was selected as the drying material. Prior to the drying

experiments, the fish samples were cleaned and salted using the same preparation procedure for all experimental conditions. The samples were stored under refrigerated conditions before testing and were allowed to equilibrate to ambient temperature before being loaded into the dryer.

For each experimental run, a total initial fish mass of 1.4 kg was used. The dimension of fish 6cmx7cmx1.5cm. The fish were distributed uniformly among the eight drying trays, corresponding to approximately 1.4 kg/tray. To reduce the influence of sample geometry on the drying kinetics, fish specimens with comparable dimensions were selected. The fish length, width, and/or thickness were maintained within 50, mm.
The initial mass of the drying load was measured using a digital weighing balance (QME, China) with a measurement accuracy of ±0.01 g. The same preparation procedure, loading arrangement, and approximate fish dimensions were maintained for the PCM and WOPCM experiments.

2.2. Solar Fish Dryer Configuration

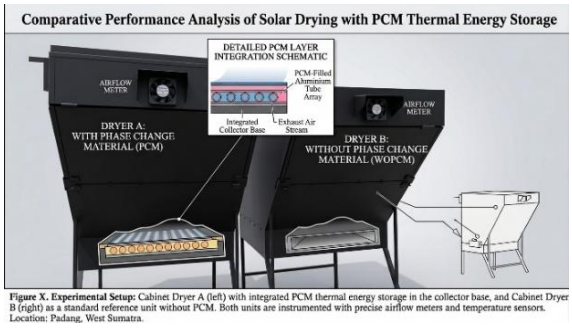
The experimental investigation was conducted using a trapezoidal direct solar fish dryer integrated with a Phase Change Material (PCM) thermal energy storage system.

The experimental system consisted of a direct solar fish dryer equipped with a solar collector, drying chamber, PCM thermal-storage unit, air inlet, and air outlet. The dryer was designed to utilize solar radiation directly for heating the drying chamber and removing moisture from the salted-fish product. The solar collector absorbed incident solar radiation and converted it into thermal energy, increasing the temperature of the air entering the drying chamber.

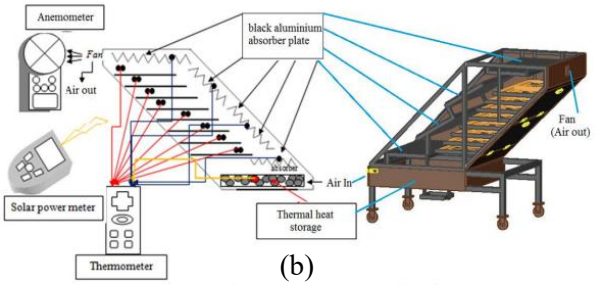
The drying chamber was constructed using carbon steel with dimensions of 1895 × 1050 × 1840 (mm). A transparent cover made of acrylic was installed to maximize solar radiation transmission into the drying chamber while allowing direct solar heating of the product. The salted-fish samples were positioned on perforated drying trays to facilitate airflow around the product and promote uniform moisture removal.

The PCM was incorporated into the drying chamber as a thermal-energy-storage medium. During periods of high solar radiation, the PCM absorbed and stored excess thermal energy through sensible and latent heat transfer. As solar radiation decreased, the stored energy was released to the surrounding air, thereby reducing the decline in drying temperature and extending the useful drying period.

A reference configuration without PCM, denoted as WOPCM, was also tested under comparable outdoor conditions. The comparison between the PCM and WOPCM configurations was used to quantify the contribution of thermal-energy storage to the overall drying performance. Figure 1 shows the schematics of solar dryer configuration.



(a)



(b)



(c)

Figure 1. Configuration of the direct solar fish dryer: (a) overall three-dimensional geometry of the dryer, (b) drying-chamber and drying-tray arrangement, and (c) location of the PCM thermal-energy-storage unit, air inlet, and air outlet.

https://doi.org/ 10.25077/metal.10.2.124-137.2026

2.3. PCM Selection and Integration

Paraffin wax was selected as the phase change material because of its suitable phase-transition temperature, relatively high latent heat, chemical stability, and non-corrosive characteristics. The thermophysical properties used in the experiment and CFD model are summarized in Table 1.

Table 1. Thermophysical properties of paraffin wax used as the PCM

Property	Symbol	Value		Unit
		Solid phase	Liquid phase	
Melting temperature	T_m	55.55		°C
Latent heat of fusion	L	190.0		kJ/kg
Density	ρ	825	755	kg/m^3
Specific heat capacity	c_p	2,200	2,100	J/(kg·K)
Thermal conductivity	λ	0.230	0.200	W/(m·K)

Source: Representative literature values reported for paraffin wax in a thermal energy storage study (Kahwaji et al., 2018).

A total PCM mass of 10 kg was used in the PCM-assisted configuration. The paraffin wax was encapsulated in steel containers/modules with dimensions of [5cmx8cm]. 16 PCM modules were arranged at the lower section of the drying chamber beneath the lowest drying tray. The modules were distributed along the airflow path so that a large portion of the external aluminum surface was exposed to the circulating drying air while maintaining sufficient free flow area for air movement through the drying chamber.

The PCM arrangement was selected to balance two competing requirements: increasing the effective heat-transfer area between the PCM enclosure and the drying air while avoiding excessive obstruction of the airflow passage. The resulting configuration therefore provides thermal contact between the PCM modules and the drying air while maintaining an open flow path toward the drying trays.

During periods of high solar radiation, the PCM absorbed thermal energy through sensible heating and phase change. When the solar radiation decreased, the stored latent heat was released as the PCM solidified, thereby reducing the rate of temperature decay inside the drying chamber.

2.4. Experimental Procedure

Experimental drying tests were conducted under natural outdoor conditions at Duri, Bengkalis. Two dryer configurations were investigated: (i) a solar dryer integrated with PCM and (ii) a solar dryer without PCM (WOPCM). The experiments were performed using salted fish prepared according to the same processing procedure to ensure consistency between the test conditions.

Before each experiment, the salted-fish samples were weighed and distributed uniformly over the drying trays. The initial mass and moisture content of the samples were recorded. The dryer was oriented toward and positioned to minimize shading from surrounding structures.

Temperature measurements were recorded at several locations, including the solar collector inlet, collector outlet, drying-chamber inlet, drying-chamber outlet, PCM surface, PCM core, and ambient environment. Solar radiation, relative humidity, and air velocity were also monitored throughout the drying process. The measurements were recorded at intervals of 30 min using a data-acquisition system.

The drying experiments were continued until the mass of the drying load became approximately constant over two consecutive measurement intervals. The constant-mass criterion was used as the experimental endpoint rather than a predetermined moisture-content value.

The reduction in fish mass was monitored at predetermined intervals using the digital weighing balance. The measurement was performed on representative samples from each tray rather than relying on a single fish specimen. The measurement procedure was kept consistent throughout the experiment.

Each experimental condition was repeated three times. Because outdoor solar drying is sensitive to changes in solar irradiance, ambient temperature, and relative humidity, the experimental runs were conducted under meteorological conditions that were as comparable as practically possible. Solar

irradiance, ambient temperature, and relative humidity were recorded for each run. These parameters were considered when interpreting differences between the PCM and WOPCM configurations. Where meteorological conditions differed between runs, the comparison was based on the corresponding time-resolved environmental conditions rather than assuming identical solar input.

2.5. Temperature and Solar Radiation Measurements

Temperature measurements were obtained using DS18B20 digital temperature sensors with an accuracy of ±0.5 °C and a resolution of 0.1 °C. A total of sixteen temperature measurement points were distributed among the solar collector, drying chamber, PCM region, and ambient environment.

The sensors were positioned at representative locations to characterize the temporal and spatial temperature distribution within the dryer. Solar irradiance was measured using a calibrated solar power meter with a resolution of 0.1 W m^{-2} and an accuracy of ±10 W m^{-2} or ±5.0%. The solar sensor was installed in an unobstructed position with its sensing surface oriented parallel to the relevant solar-exposure plane so that the measured value represented the incident solar irradiance received by the dryer.

Ambient temperature and relative humidity were simultaneously measured using a digital thermo-hygrometer (HTC-2, Taffware). Fish mass was monitored using a digital weighing balance (AR991, Huber) with a resolution of 0.01 g.

All measurement instruments were checked before the experiments. The temperature sensors were positioned so that they did not significantly obstruct the airflow or alter the local heat-transfer characteristics inside the dryer

2.6. Determination of Moisture Content and Moisture Ratio

The moisture content of the salted-fish samples was determined from the measured sample mass during the drying process. The moisture content on a wet basis was calculated as:

$$MC_{wb} = \frac{m_w}{m} \times 100 \qquad (1)$$

where $m_w$is the mass of water contained in the sample (kg) and mis the total sample mass (kg).
The moisture ratio (MR) was calculated according to:

$$MR = \frac{M_t - M_e}{M_0 - M_e} \qquad (2)$$

where $M_t$is the moisture content at drying time t, $M_0$is the initial moisture content, and $M_e$is the equilibrium moisture content.

Because the equilibrium moisture content was small relative to $M_t$and M_0under the drying conditions considered in this study, the simplified form was used:

$$MR = \frac{M_t}{M_0} \qquad (3)$$

The simplified expression was used consistently for comparison of the drying kinetics of the PCM and WOPCM configurations.

The moisture-content and moisture-ratio calculations were based on the measured mass of the drying material at each measurement interval. The use of the simplified moisture-ratio expression is subject to the assumption that $M_e$is sufficiently small relative to the measured moisture contents.

2.7. Specific Moisture Extraction Rate

The specific moisture extraction rate (SMER) was used to evaluate the effectiveness of energy utilization during the drying process. SMER represents the amount of moisture removed per unit of energy supplied to the drying system and was calculated as:

$$SMER = \frac{\Delta m_w}{E_{in}} \qquad (4)$$

where $\Delta m_w$is the total mass of moisture removed (kg) and $E_{in}$is the total incident solar energy supplied to the dryer (kWh).

 https://doi.org/ 10.25077/metal.10.2.124-137.2026

The incident solar energy was calculated by integrating the measured solar irradiance over the effective collector/drying area and drying period:

$$E_{in} = \frac{A}{1000}\int_0^t G\,(t)\,dt \qquad (5)$$

where Ais the solar-receiving area (m²), G(t)is the measured solar irradiance (W m⁻²), and tis the drying duration (h). The calculated energy therefore represents the solar radiation incident on the receiving area rather than only the useful thermal energy transferred to the drying air. A higher SMER indicates that a greater quantity of moisture was removed per unit of incident solar energy.

2.10. CFD Model Development

A two-dimensional CFD model of the solar fish dryer was developed using the finite-volume method to investigate the coupled airflow and heat-transfer behavior inside the drying chamber. The computational domain reproduced the main geometrical features of the experimental dryer, including the solar collector, drying chamber, drying trays, air inlet and outlet, and PCM region.

The primary purpose of the CFD model was not simply to reproduce the experimentally measured temperatures. Because the experimental measurements were obtained at discrete sensor locations, the CFD model was used to provide spatially resolved information on airflow velocity, temperature distribution, thermal gradients, flow acceleration, recirculation, and potential low-velocity regions throughout the drying chamber. The simulations were also used to examine the interaction between the PCM configuration and the airflow path and to identify whether PCM placement could introduce flow obstruction or thermal non-uniformity.

The CFD results were therefore used to interpret the experimental observations and to provide design-related information that cannot be obtained directly from the experimental sensor measurements alone.

2.11. Turbulence and PCM Modelling

The turbulence behavior of the airflow was modeled using the realizable turbulence model with appropriate near-wall treatment. This model was selected because of its suitability for buoyancy-driven and internal airflow applications.

The PCM phase-change process was modeled using the enthalpy-porosity method. The total PCM enthalpy was expressed as:

$$H = h + f_l L \qquad (6)$$

where His the total enthalpy, his the sensible enthalpy, $f_l$is the liquid fraction, and Lis the latent heat of fusion. The liquid fraction was defined as a temperature-dependent function over the PCM melting range.

For temperatures below the solidus temperature T_s, the liquid fraction was set to zero; for temperatures above the liquidus temperature T_l, the liquid fraction was set to unity. Within the phase-change interval, the liquid fraction was assumed to vary linearly with temperature:

$$f_l = \begin{cases} 0, & T < T_s \\ \dfrac{T - T_s}{T_l - T_s}, & T_s \le T \le T_l \\ 1, & T > T_l \end{cases} \qquad (7)$$

The mushy-zone formulation was applied to represent the reduction in PCM fluid motion during solidification.

2.12. Boundary Conditions

The solar collector was subjected to a measured solar heat flux corresponding to the experimental solar radiation conditions. The ambient temperature was imposed at the external boundaries, while the air inlet was specified according to the experimentally measured airflow condition.

At the dryer outlet, a pressure-outlet boundary condition was applied. The walls of the dryer were modeled using appropriate thermal boundary conditions based on the material properties and measured external temperatures. The PCM was initially assigned its experimentally measured temperature, while its thermophysical properties, including density, thermal conductivity, specific heat, melting temperature, and latent heat, were incorporated into the model.

The transient CFD simulations were performed using the same solar-radiation and ambient-temperature profiles measured during the experimental tests, allowing direct comparison between numerical and experimental results.

2.13. Mesh Independence and Time-Step Sensitivity

The simulation was performed using a time step of 1 s over a total flow time of 1000 s (1000-time steps), with a maximum of 20 iterations per time step. This configuration was selected to ensure numerical stability while adequately resolving the transient thermal response of the drying chamber. Convergence at each time step was confirmed through residual monitoring, with absolute convergence criteria of 0.001 for continuity and momentum equations and 1×10^{-6} for the energy equation. All monitored residuals (continuity: 7.37×10^{-7}; x-velocity: 4.80×10^{-8}; y-velocity: 3.90×10^{-8}; energy: 2.84×10^{-13}) satisfied these criteria at the final time step, confirming solution convergence

2.14. Comparative Performance Evaluation

The thermal and drying performance of the PCM-assisted dryer was compared with that of the WOPCM dryer. The comparison included drying temperature, temperature uniformity, drying time, moisture ratio, drying rate, thermal efficiency, specific moisture extraction rate, and the ability of the system to maintain the drying temperature during periods of reduced solar radiation.

The CFD results were further used to visualize the temperature contours, velocity fields, airflow trajectories, and thermal gradients within the dryer. These results provided additional insight into the mechanisms responsible for the experimentally observed performance improvement associated with PCM integration.

Particular attention was given to the PCM's ability to reduce temperature fluctuations and maintain a more stable drying environment after solar radiation decreased. This combined experimental–numerical approach enabled the influence of PCM integration on both the macroscopic drying performance and the internal heat-transfer and airflow characteristics of the dryer to be systematically evaluated

3. RESULTS AND DISCUSSION

The results demonstrate the drying behavior of salted fish under solar exposure, with particular emphasis on changes in moisture content and sample mass over time. The observed trends provide insight into moisture removal dynamics and the effectiveness of solar drying throughout the process.

The solar irradiance profile exhibited substantial temporal variability throughout the drying experiment. As shown in Figure 2 the solar irradiance ranging from approximately 155 to 715 W m^{-2}. Irradiance remained relatively low during the initial 0–1 h (~155 W m^{-2}) before increasing sharply to a maximum of 715 W m^{-2} at approximately 2.4 h, indicating a period of intense solar energy availability. Thereafter, irradiance declined to ~270 W m^{-2} at 4.3 h, followed by a secondary increase to ~530 W m^{-2} at 6.4 h before decreasing again toward the end of the experiment. This pronounced fluctuation reflects the dynamic nature of solar energy input, potentially associated with changes in cloud cover, atmospheric conditions, and solar position, and provides an important explanation for the non-monotonic moisture-loss behavior observed during drying. In particular, periods of higher irradiance likely enhanced heat transfer and moisture evaporation, whereas reduced irradiance would have lowered the available energy for evaporation.

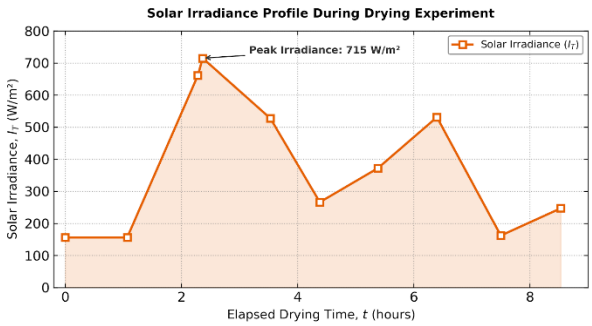


Figure 2. Variation in solar irradiance during the drying experiment

Figure 3 illustrates the real-time temperature-monitoring system used to characterize the spatial

https://doi.org/ 10.25077/metal.10.2.124-137.2026

thermal distribution within the drying chamber. The dual-node ESP32-based data acquisition system enabled simultaneous monitoring of multiple thermistor locations distributed across the drying racks.

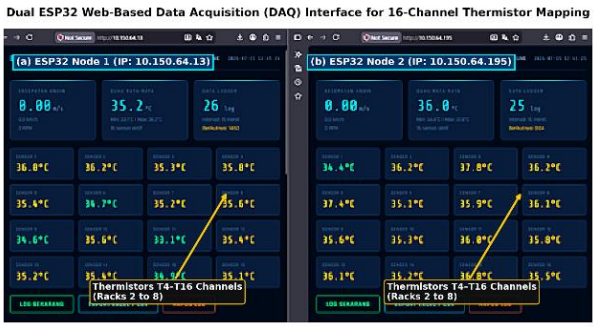


Figure 3. ESP32-based web data-acquisition interface used for real-time monitoring of temperature distribution at multiple locations within the solar dryer.

At the measurement instant shown, the average temperatures recorded by Nodes 1 and 2 were approximately 35.2 and 36.0 °C, respectively. The corresponding temperature ranges were 33.1–36.2 °C and 34.4–37.4 °C, indicating a spatial temperature variation of approximately 3 °C across the monitored locations. These multi-point measurements provide experimental evidence of the spatial thermal behavior of the dryer and serve as an important basis for validating the CFD-predicted temperature distribution.

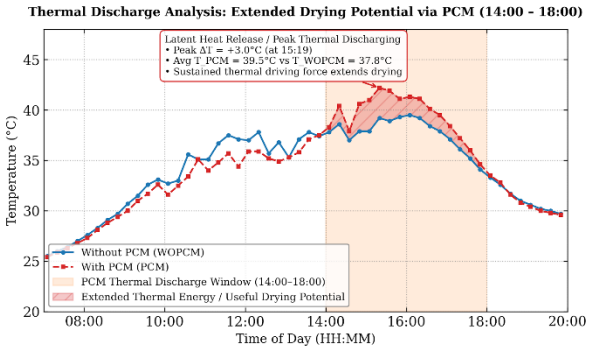


Figure 4 Thermal performance curves of the test cells with and without phase change material (PCM)

Figure 4 presents the thermal response of the dryer with and without PCM during the drying period. Both configurations exhibited a similar sensible-heating trend during the period of increasing solar irradiance. However, differences became more evident during the subsequent period of decreasing solar radiation. During the four-hour discharge interval, the PCM-assisted system maintained a higher mean temperature of approximately 39.02°C compared with 37.35°C for the WOPCM configuration. This difference indicates that the PCM released stored thermal energy during the period of decreasing solar input and thereby reduced the rate of temperature decay.

The observed behavior is consistent with the expected operation of latent heat storage. During periods of high solar radiation, part of the available thermal energy was stored in the PCM. When solar input decreased, the stored energy was released during PCM solidification, allowing the drying chamber to maintain a higher temperature than the WOPCM configuration. Therefore, the primary contribution of PCM in the present system was thermal buffering and extension of the effective drying period rather than a substantial increase in the maximum daytime temperature.

Figure 5 illustrates the variation in salted-fish moisture content during the solar drying process. Overall, the moisture content decreased from approximately 55% at the beginning of drying to approximately 14% after 6–7 h, indicating substantial moisture removal. However, the experimental drying curve exhibited distinct non-monotonic behavior, characterized by temporary increases in moisture content during the intermediate and final stages of drying. These moisture-regain events are likely associated with fluctuations in the drying environment, particularly reductions in drying-air temperature and increases in ambient relative humidity during periods of declining solar irradiance. Such behavior highlights an important limitation of conventional solar drying, in which the moisture-removal driving force can deteriorate when solar energy availability decreases.

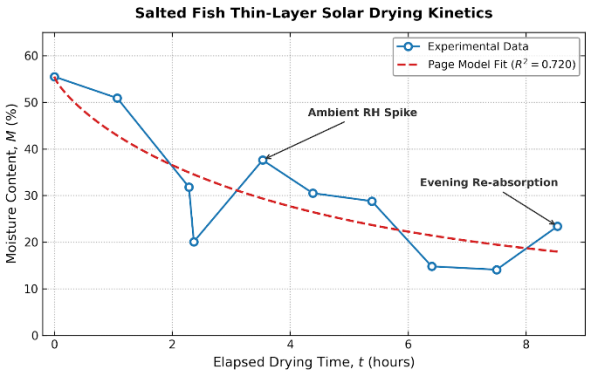


Figure 5. Variation in salted-fish moisture content during the solar drying process.

The drying kinetics were further evaluated using the Page model, expressed as:

$$MR = \exp(-kt^n) \qquad (8)$$

where $MR$is the moisture ratio, $t$is the drying time (h), $k$is the empirical drying-rate constant, and $n$is the dimensionless empirical drying exponent. Based on the experimental data, the fitted Page model parameters were approximately $k = 0.235$ h^{-n}and $n = 0.753$, with a coefficient of determination of approximately $R^2 = 0.72$. The fitted curve provides an empirical representation of the overall reduction in moisture ratio during drying. However, the deviations between the experimental data and the fitted curve are associated with fluctuations in drying conditions, particularly changes in ambient relative humidity and moisture re-absorption during the later stages of drying.

The Page model provides a useful description of the overall drying trend; however, the non-monotonic behavior observed at some stages indicates that the drying process was affected by changes in the external drying conditions. In particular, variations in solar irradiance, drying-air temperature, and ambient relative humidity can temporarily alter the moisture-transfer driving force. Therefore, the Page-model fit should be interpreted as an empirical representation of the overall drying kinetics rather than as a complete description of the short-term fluctuations in moisture content.

Figure 6 presents the simultaneous changes in moisture content and sample mass during approximately 9 h of solar drying. The overall trends are consistent with moisture removal: the moisture content decreased from approximately 55% at the beginning of drying to a minimum of approximately 14–15% after 7–8 h, while the sample mass decreased from approximately 1.60 to 1.00 kg. The corresponding reduction in total mass was approximately 37–38%.

As expected, the general trends of moisture content and sample mass are related because water loss constitutes a major component of the total mass reduction. However, short-term deviations from a strictly monotonic relationship were observed during some periods of the experiment. In particular, temporary increases in the calculated moisture content do not necessarily imply a corresponding increase in the total sample mass.

These deviations should therefore be interpreted cautiously. Possible mechanisms include moisture redistribution within the fish matrix, moisture adsorption or desorption associated with changes in ambient relative humidity, non-uniform moisture distribution among the fish samples, and measurement uncertainty. Changes in drying-air temperature and ambient relative humidity can also alter the instantaneous moisture-transfer driving force. Because the present study did not independently measure moisture distribution within individual fish or conduct a sorption-isotherm experiment, the precise mechanism responsible for each short-term fluctuation cannot be established conclusively.

Nevertheless, the simultaneous reduction in total sample mass and overall moisture content demonstrates that evaporative moisture removal was the dominant process over the complete drying period. The initial rapid reduction is consistent with the removal of more readily available moisture, whereas the slower reduction during the later stage indicates increasing resistance to internal moisture migration as the fish became progressively dehydrated

 https://doi.org/ 10.25077/metal.10.2.124-137.2026

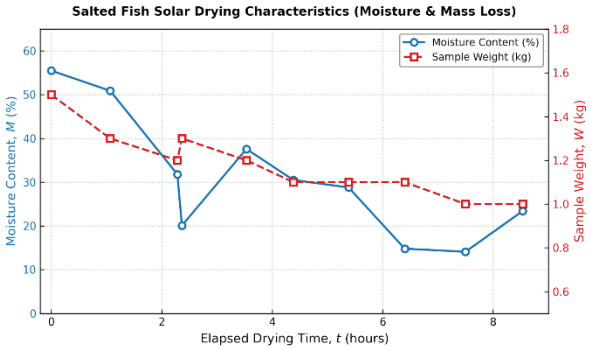


Figure 6. The changes in moisture content and sample mass of salted fish.

The dried fish obtained using the solar dryer with PCM exhibited a better overall product appearance than that obtained using the WOPCM system, as shown in Figure 7. The PCM-treated fish showed a more desirable and uniform dried appearance, indicating that the incorporation of PCM may have provided more favorable thermal conditions for producing a higher-quality dried fish product.



PCM WOPCM

Figure 7. Dried fish texture using the solar dryer with PCM vs WOPCM

The dried fish obtained using the solar dryer with PCM exhibited a visually more uniform appearance than the product obtained using the WOPCM configuration, as shown in Figure 7. The PCM-treated samples appeared more uniform in surface appearance and drying condition. However, visual appearance alone is insufficient to establish overall product quality. Important quality indicators for dried fish include final moisture content, water activity, texture, microbial quality, color, and other physicochemical characteristics. Because these parameters were not comprehensively measured in the present study, the observed difference in appearance is reported only as a qualitative observation and should not be interpreted as conclusive evidence that PCM produced a higher-quality product. A quantitative assessment of these quality attributes is recommended for future work

Figure 8 Represents the static temperature field $T[\mathrm{K}]$ with a legend range of 300.0 K (3.000×10^2 K) to 341.3 K (3.413×10^2 K). The thermal domain exhibits a smooth, monotonic decay along the primary flow path from the top boundary down to the lower right corner.

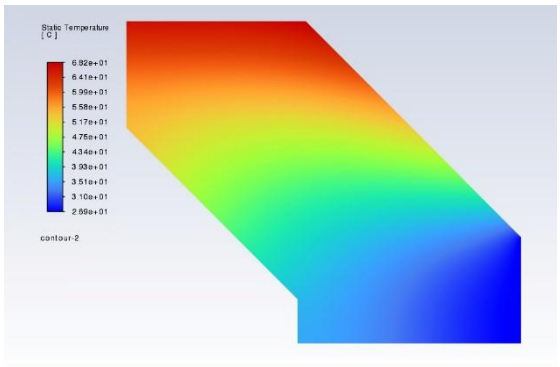


Figure 8. Temperature distribution of solar drier

Figure 9 and 10 show the CFD results provide spatial information that cannot be obtained from the discrete experimental temperature measurements alone. The velocity contours indicate that the airflow is non-uniform within the drying chamber, with localized high-velocity regions near flow restrictions and lower-velocity regions in areas where the flow expands or separates. These low-velocity regions are important because they may reduce convective heat and mass transfer and consequently contribute to spatial differences in drying conditions among the trays.

The temperature field shows the corresponding thermal response of the airflow. Regions with stronger airflow exhibit enhanced convective transport, whereas low-velocity or recirculation regions can exhibit different thermal behaviour because of reduced advective transport. The CFD results therefore provide a mechanistic explanation for the spatial temperature variation observed experimentally.

Importantly, the CFD model also allows the influence of the PCM configuration on the airflow path to be evaluated. The PCM should provide sufficient heat-transfer surface area for thermal charging and discharging while avoiding excessive blockage of the flow passage. Thus, the CFD analysis provides design information regarding the trade-off between thermal-storage effectiveness and airflow resistance, which cannot be determined from the experimental temperature measurements alone.

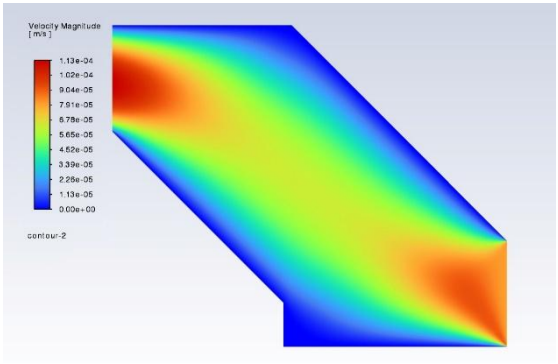


Figure 9. Velocitiy distrubition inside dryer

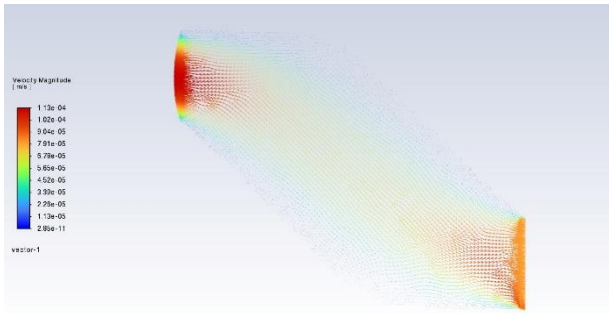


Figure 10 Velocity distribution

Physical Interpretation and Validity

Flow Field Dynamics: The velocity distribution indicates ultra-low speed, low Reynolds number laminar regime flow ($Re \ll 1$), typical of natural convection or micro-ventilation channels. The velocity boundary layer growth is clearly visible, vanishing to zero at solid walls. Acceleration near the entrance and exit is consistent with mass conservation across geometric contractions ($\dot{m} = \rho A u = \text{const}$).

Thermal-Fluid Coupling: The temperature contours show an advective-conductive balance. Isotherms deform parabolically along the primary flow direction, following the high-velocity core identified in Figure 2. Near the bottom-right corner, low velocities coincide with a uniform low-temperature zone ($300.0 - 304.1$ K), indicating convective dissipation into a cooler sink.

Flow Separation & Stagnation: A secondary low-velocity zone ($< 1.131 \times 10^{-5}$ m s^{-1}) forms in the bottom horizontal pocket, corresponding to a stagnation region where momentum transport drops significantly.

Numerical Convergence & Stability Assessment

Mesh Continuity & Smoothness: The smooth gradient transitions without jagged contour steps suggest a sufficiently fine cell resolution along the core flow path. However, numerical diffusion appears subtle along the angled wall bounds.

Potential Boundary Anomalies: In Figure 2, velocity gradients at the upper left boundary show sharp spatial changes right at the inlet corner, which can indicate unrefined inflation layer meshing or artificial pressure inlet boundary effects.

Continuity Balance: The velocity magnitude drop in the central angled duct section suggests flow expansion, but without pressure contour or residual history verification, mass conservation across the angled elbow requires quantitative flux auditing.

The experimental results demonstrate that the integration of Phase Change Material (PCM) significantly influenced the thermal behavior of the direct solar fish dryer by extending the effective drying period. Rather than functioning as an additional heat source, the PCM acted as a latent thermal energy storage medium that absorbed surplus solar energy during periods of high solar irradiance and gradually released the stored energy when solar radiation decreased. Consequently, the drying chamber maintained a more stable thermal environment after peak solar hours, allowing the drying process to continue for a longer duration than the system without PCM (WOPCM). This observation indicates that PCM integration improves the continuity of thermal energy supply instead of merely increasing the peak drying temperature.

The extended drying period can be explained by the thermophysical characteristics of paraffin wax, which possesses a relatively high latent heat of

 https://doi.org/ 10.25077/metal.10.2.124-137.2026

fusion and undergoes a phase transition at an approximately constant temperature. During daytime operation, a portion of the absorbed solar energy was utilized to increase the sensible temperature of the drying air, while another portion was stored within the PCM as latent heat during the melting process. Once the available solar radiation decreased, the molten paraffin gradually solidified and released the stored latent heat to the surrounding air. This delayed heat release reduced the cooling rate inside the drying chamber and maintained a higher air temperature compared with the dryer operated without PCM. As a result, the driving force for moisture evaporation from the salted fish was sustained for a longer period, thereby extending the effective drying operation.

From a heat transfer perspective, the PCM altered the transient thermal response of the drying system by increasing its overall thermal inertia. The stored latent heat compensated for the reduction in solar energy input during late afternoon and cloudy conditions, resulting in a slower decline in chamber temperature. Although the instantaneous drying rate during the charging period may not have been significantly higher than that of the conventional dryer, the accumulated drying duration increased because useful thermal energy remained available after direct solar heating diminished. This behavior is particularly advantageous for drying fish products, where maintaining a relatively stable drying temperature is essential to minimize thermal stress, prevent case hardening, and promote uniform moisture diffusion throughout the product.

The present findings are consistent with previous investigations reporting that PCM-assisted solar dryers enhance thermal stability by extending drying operation beyond sunset and reducing temperature fluctuations. Studies by Ebrahimi et al. (2021) demonstrated that latent heat storage effectively prolonged useful drying time while improving thermal efficiency. Similarly, Andharia et al. (2022) reported that paraffin-based PCM systems maintained higher chamber temperatures during low solar radiation periods, thereby improving overall dryer performance. Karaağaç et al. (2021) further emphasized that latent heat storage contributes to more stable thermal conditions by minimizing the influence of fluctuating solar irradiance. The present experimental results reinforce these findings by demonstrating that paraffin wax integrated into a trapezoidal direct solar fish dryer effectively sustained drying temperatures under practical operating conditions.

It should be noted, however, that the integration of PCM does not necessarily accelerate the initial drying stage. During periods of intense solar radiation, a fraction of the incoming thermal energy was absorbed by the paraffin wax to initiate melting rather than directly heating the drying air. Consequently, the initial chamber temperature increase may have been slightly lower than that observed in the dryer without PCM. Nevertheless, this temporary reduction in sensible heating was compensated by the subsequent release of latent heat during the discharge process, resulting in superior thermal stability throughout the latter stages of drying. Such behavior is characteristic of latent heat storage systems and should therefore be considered an inherent design feature rather than a performance deficiency.

Several limitations should also be acknowledged. The charging and discharging characteristics of paraffin wax depend strongly on solar radiation intensity, ambient temperature, PCM mass, and the geometric configuration of the storage compartment. Under prolonged periods of low solar irradiance, the PCM may not completely melt, thereby reducing the amount of thermal energy available during the discharge stage. In addition, the relatively low thermal conductivity of paraffin wax may limit heat transfer between the PCM and the circulating drying air, potentially decreasing the overall effectiveness of thermal energy recovery.

Future investigations should therefore evaluate the influence of PCM mass, encapsulation geometry, fin-assisted heat transfer enhancement, and alternative high-conductivity composite PCMs on the thermal performance of direct solar dryers. Furthermore, long-term cyclic thermal performance should be examined to assess the durability and

reliability of PCM-assisted drying systems under repeated daily operating conditions.

Overall, the experimental evidence confirms that integrating paraffin wax as a latent heat storage medium enhances the thermal stability of the direct solar fish dryer by extending the effective drying period rather than increasing the maximum drying temperature. This improved thermal continuity is expected to contribute to more consistent drying conditions, better product quality, and greater utilization of renewable solar energy, thereby supporting the development of sustainable drying technologies for small-scale fish processing industries.

4. CONCLUSION

This study experimentally evaluated the thermal performance of an direct trapezoidal solar fish dryer integrated with paraffin wax as a Phase Change Material (PCM). The results demonstrated that PCM effectively stored excess solar thermal energy during periods of high solar radiation and gradually released the stored heat when solar intensity decreased, thereby maintaining a more stable drying chamber temperature and extending the effective drying period. Compared with the dryer without PCM, the PCM-assisted system exhibited improved thermal stability and reduced temperature fluctuations, indicating its potential to enhance the reliability of solar drying under variable weather conditions. These findings suggest that PCM integration is a promising strategy for improving renewable-energy-based fish drying systems. Future work should focus on optimizing PCM quantity and placement, evaluating drying kinetics and product quality, and assessing long-term thermal performance under different climatic conditions.

ACKNOWLEDGEMENT

The authors gratefully acknowledge the financial support provided by the Ministry of Higher Education, Science and Technology of the Republic of Indonesia through the research grant under contract number 269/C3/DT.05.00/PL-Baru/2026. The support provided has been invaluable for the successful completion of this research.

REFERENCES

[1] P. K. S. Rathore and B. S. Sikarwar, “Thermal energy storage using phase change material for solar thermal technologies: A sustainable and efficient approach,” *Sol. Energy Mater. Sol. Cells*, vol. 277, no. June, 2024.

[2] M. O. Karaağaç, A. Ergün, Ü. Ağbulut, A. E. Gürel, and İ. Ceylan, “Experimental analysis of CPV/T solar dryer with nano-enhanced PCM and prediction of drying parameters using ANN and SVM algorithms,” *Sol. Energy*, vol. 218, no. September 2020, pp. 57–67, 2021.

[3] J. K. Andharia, B. Markam, D. Dzhonova, and S. Maiti, “A comparative performance analysis of sensible and latent heat based storage in a small-scale solar thermal dryer,” *J. Energy Storage*, vol. 45, no. September 2021, p. 103764, 2022.

[4] H. Ebrahimi, H. Samimi Akhijahani, and P. Salami, “Improving the thermal efficiency of a solar dryer using phase change materials at different position in the collector,” *Sol. Energy*, vol. 220, no. April, pp. 535–551, 2021.

[5] P. Mirzaee, P. Salami, H. Samimi Akhijahani, and S. Zareei, “Life cycle assessment, energy and exergy analysis in an indirect cabinet solar dryer equipped with phase change materials,” *J. Energy Storage*, vol. 61, no. August 2022, p. 106760, 2023.

[6] B. Brahma, A. K. Shukla, and D. C. Baruah, “Energy, exergy, economic and environmental analysis of phase change material based solar dryer (PCMSD),” *J. Energy Storage*, vol. 88, no. March, p. 111490, 2024.

[7] J. Feng *et al.*, “Aligned channel Gelatin@nanoGraphite aerogel supported form-stable phase change materials for solar-thermal energy conversion and storage,” *Carbon N. Y.*, vol. 201, no. September 2022, pp. 756–764, 2023.

[8] J. Assadeg, A. H. A. Al-Waeli, A. Fudholi, and K. Sopian, “Energetic and exergetic analysis of a new double pass solar air collector with fins and phase change material,” *Sol. Energy*, vol. 226, no. August, pp. 260–271, 2021.

[9] W. Hu, A. V. Nickolaevich, Y. Du, and C. Hou, "Design and thermal performance evaluation of the thermal storage layer of a solar air collector with comprehensive consideration of six factors of phase-change materials," *J. Energy Storage*, vol. 90, no. PA, p. 111888, 2024.

[10] S. Manikandan, G. Muthuvairavan, M. Samykano, and S. K. Natarajan, "Numerical simulation of various PCM container configurations for solar dryer application," *J. Energy Storage*, vol. 86, no. PB, p. 111294, 2024.

[11] M. C. Gilago and V. P. Chandramohan, "Performance parameters evaluation and comparison of passive and active indirect type solar dryers supported by phase change material during drying ivy gourd," *Energy*, vol. 252, p. 123998, 2022.

[12] S. Nižetić, M. Jurčević, D. Čoko, M. Arıcı, and A. T. Hoang, "Implementation of phase change materials for thermal regulation of photovoltaic thermal systems: Comprehensive analysis of design approaches," *Energy*, vol. 228, 2021.

[13] H. Atalay and E. Cankurtaran, "Energy, exergy, exergoeconomic and exergo-environmental analyses of a large scale solar dryer with PCM energy storage medium," *Energy*, vol. 216, p. 119221, 2021.

[14] D. Chaatouf, A. G. Ghiaus, and S. Amraqui, "Optimization of a solar air heater using a phase change material for drying applications," *J. Energy Storage*, vol. 55, no. PB, p. 105513, 2022.

[15] R. Sehrawat, R. K. Sahdev, D. Chhabra, and S. Tiwari, "Experimentation and optimization of phase change material integrated passive bifacial photovoltaic thermal greenhouse dryer," *Sol. Energy*, vol. 257, no. February, pp. 45–57, 2023.

[16] Q. Guo, H. Yi, F. Jia, and S. Song, "Design of MoS2/MMT bi-layered aerogels integrated with phase change materials for sustained and efficient solar desalination," *Desalination*, vol. 541, no. August, p. 116028, 2022.

[17] L. Luo *et al.*, "Form-stable phase change materials based on graphene-doped PVA aerogel achieving effective solar energy photothermal conversion and storage," *Sol. Energy*, vol. 255, no. February, pp. 146–156, 2023.